

θ vacuum effects on the chiral condensation and the η' meson correlators in the two-flavor massive QED₂ on the lattice

Hidenori Fukaya and Tetsuya Onogi

Yukawa Institute for Theoretical Physics, Kyoto University, Kyoto 606-8502, Japan

We study the scalar and pseudoscalar condensations and the η' meson correlators of the two-flavor massive Schwinger model in the $\theta \neq 0$ vacuum. Exploiting our new method which was developed to investigate topological effects in the previous work, we find that $\langle \bar{\psi}\gamma_5\psi \rangle^\theta \neq 0$ and there exists a long-range correlation of the η' meson. This phenomenon is well described by the clustering property. We also find that even in $\theta = 0$ case the cancellation of the long-range correlation is nontrivial and requires accurate contributions from higher topological sectors. Our results imply that the fluctuation of the “disconnected” diagram originates from the pseudoscalar condensation in each topological sector.

I. INTRODUCTION

The topological structure is one of the essential aspects of the gauge theory. In addition to its theoretical importance, it has phenomenological implications in particle physics such as the η' meson mass and the θ vacuum in QCD. Although much is known in the instanton dilute gas approximation, in order to go beyond the level of qualitative understanding truly nonperturbative studies are required. For such purposes the lattice gauge theory should serve as a powerful tool, it has, however, been a nontrivial task to reproduce the topological structure since the naive lattice action does not preserve such properties.

Recently a new formulation of the lattice action, the Ginsparg-Wilson fermion [1], which realizes the exact chiral symmetry and the chiral anomaly has been proposed. Thus it would be an opportunity for the lattice gauge theory to provide a quantitative study of the topological structure of the gauge theories using this new formalism.

In this work we study the $n_f = 2$ massive Schwinger model using this new lattice formalism and the method developed in our previous work [2]. From the analytical studies of this model in the continuum space [3, 4, 5, 6, 7, 8, 9], it has been found that the pion mass and the chiral condensates at strong coupling and small θ behave as

$$\begin{aligned} m_\pi^\theta &= c_\pi m^{2/3} g^{1/3} \cos^{2/3} \frac{\theta}{2}, \\ -\langle \bar{\psi}\psi \rangle^\theta &= c_{\bar{\psi}\psi} m^{1/3} g^{2/3} \cos^{4/3} \frac{\theta}{2}, \\ i\langle \bar{\psi}\gamma_5\psi \rangle^\theta &= c_{\bar{\psi}\psi} m^{1/3} g^{2/3} \sin \frac{\theta}{2} \cos^{1/3} \frac{\theta}{2}, \end{aligned} \quad (1)$$

where g denotes a gauge coupling constant, m is the fermion mass, $\gamma_5 = \text{diag}(1, -1)$ and $c_\pi, c_{\bar{\psi}\psi}$ are numerical constants. Although there has been extensive lattice studies on the massive Schwinger model, they are limited to the scalar condensation $\langle \bar{\psi}\psi \rangle$ and the η' meson masses in the $\theta = 0$ vacuum [10, 11, 12, 13, 14, 15, 16, 17, 18]. The lattice studies for the $\theta \neq 0$ vacuum done so far are only those in the pure U(1) gauge theory [20, 21, 22, 23, 24, 25, 26].

Our goal is to compute the scalar and the pseudoscalar condensations $\langle \bar{\psi}\psi \rangle, \langle \bar{\psi}\gamma_5\psi \rangle$ as well as the η' meson correlators $\langle \eta'^\dagger \eta' \rangle$ for fixed topological charges and study how the practical lattice calculations reproduce physical quantities in the θ vacuum.

In section II, we explain our method of simulations and how to evaluate the θ vacuum effects by reweighting. The results of the chiral condensation are presented in section III. The connection between the η' correlators and the chiral condensations in each sector are shown in section IV. In section V, we also present our result of the η' meson correlators in the θ vacuum. The summary and the discussion are given in section VI. Appendix is devoted to the study of the topological susceptibility.

II. MONTE CARLO SIMULATIONS AND THE REWEIGHTING

In this section, we briefly explain our method of the simulation. More details can be found in our previous paper [2]. We take the gauge action proposed by Lüscher [27] and the domain-wall fermion action [28, 29],

$$\begin{aligned} S &= \beta S_G + S_F, \quad (2) \\ S_G &= \begin{cases} \sum_P \frac{(1 - \text{Re}P_{\mu\nu}(x))}{1 - (1 - \text{Re}P_{\mu\nu}(x))/\epsilon} & \text{if admissible} \\ \infty & \text{otherwise} \end{cases}, \quad (3) \\ S_F &= \sum_{x,x'} \sum_{s,s'} \sum_{i=1}^2 [\bar{\psi}_s^i(x) D_{DW}(x, s; x', s') \psi_{s'}^i(x') \\ &\quad + \phi_s^{i*}(x) D_{AP}(x, s; x', s') \phi_{s'}^i(x')], \quad (4) \end{aligned}$$

where $\beta = 1/g^2$, $P_{\mu\nu}$ denotes the plaquette, ϕ 's are Pauli-Villars regulators which cancel the bulk contribution of the domain-wall fermions and ϵ is a fixed constant. The gauge fields generated by this action satisfy Lüscher's bound;

$$1 - \text{Re}P_{\mu\nu}(x) < \epsilon \quad \text{for all } x, \mu, \nu. \quad (5)$$

Those gauge fields which satisfy the above condition are called “admissible”. The “admissible” gauge fields have

an exact topological charge defined as

$$Q \equiv \sum_x \frac{-i}{4\pi} \epsilon_{\mu\nu} \ln P_{\mu\nu},$$

on the lattice if $\epsilon < 2$. This charge is never changed in the evolution in the hybrid Monte Carlo algorithm so that we can evaluate the observables in each sector separately. We take a 16×16 ($\times 6$) lattice at $\beta = 1.0$ and $\epsilon = 1.0$. Fermion mass is chosen as $m = 0.1, 0.15, 0.2, 0.25, 0.3$. Fifty molecular dynamics steps with a step size $\Delta\tau = 0.035$ are performed in one trajectory. Configurations are updated every 10 trajectories. For each topological sector, around 500 trajectories are taken for the thermalization starting from the initial configuration which is the classical instanton solution with topological charge Q . We generate 300 configurations for each sector for the measurements and from 1000 to 10000 for the reweighting factors at various β .

The expectation value of an operator O in the θ vacuum is expressed as

$$\langle O \rangle_{\beta, m}^{\theta} = \frac{\sum_{Q=-\infty}^{+\infty} e^{iQ\theta} \langle O \rangle_{\beta, m}^Q R^Q(\beta, m)}{\sum_{Q=-\infty}^{+\infty} e^{iQ\theta} R^Q(\beta, m)}, \quad (6)$$

where $\langle \cdot \rangle_{\beta, m}^Q$ denotes the expectation value in the sector with Q at β, m and R^Q is the reweighting factor;

$$\begin{aligned} R^Q(\beta, m) &= \frac{Z_Q(\beta, m)}{Z_0(\beta, m)} \\ &= e^{-\beta S_G^Q} \times \text{Det}^Q \times e^{\int_{\beta}^{\infty} d\beta' \Delta S^Q(\beta', m)} \end{aligned} \quad (7)$$

where Z_Q is the partition function in each sector, Det^Q denotes the contribution from fermion determinants in the classical background with topological charge Q and S_G^Q is the action of the background. Det^Q 's are calculated by the Householder method and the QL method. The integrals of ΔS^Q which is defined as

$$\Delta S^Q(\beta', m) \equiv \langle S_G - S_G^Q \rangle_{\beta', m}^Q - \langle S_G \rangle_{\beta', m}^0, \quad (8)$$

are evaluated by fitting the data with polynomials (See Fig. 1);

$$\Delta S^Q(\beta', m) = \frac{a_1}{\beta'^2} + \frac{a_2}{\beta'^3}. \quad (9)$$

We present the Q dependence of R^Q in Fig. 2 and in Table I. The plots are consistent with the behavior indicated by the Atiyah-Singer index theorem. In Fig.3 we show the lowest 20 eigenvalues with positive or negative chiralities of the massless Domain-wall Dirac operator for a typical configuration in each topological sector. The smallest eigenvalues are consistent with exact zero at $O(10^{-3})$, which suggests that the index theorem is realized very well due to the smallness of the violation of chiral symmetries. As Fig.2 indicates, we can ignore the contribution from large Q sectors. We evaluated the total expectation values by summing $-4 \leq Q \leq 4$ sectors for $m = 0.1, 0.15, 0.2$ and $-5 \leq Q \leq 5$ sectors for $m = 0.25, 0.3$.

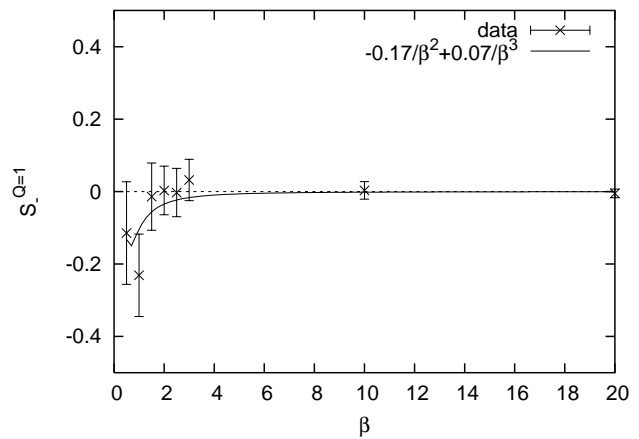


FIG. 1: Plot of $\Delta S^{Q=1}(\beta, m = 0.2)$. The solid line shows the result of the fit. ($a_1 = -0.17, a_2 = 0.07, \chi^2/\text{dof} = 1.4, \int_{\beta=1.0}^{\infty} d\beta' \Delta S^1(\beta', m) = -0.14(11)$).

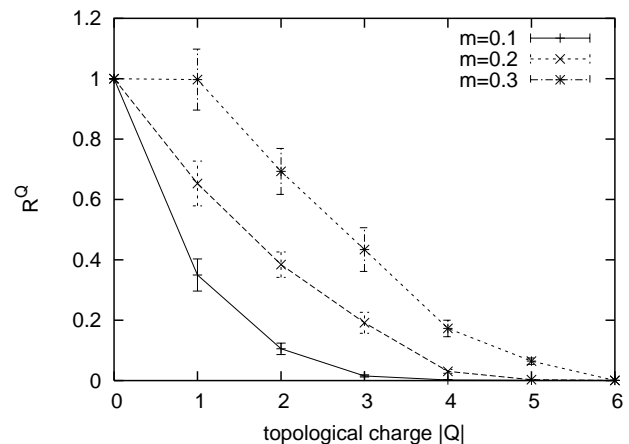


FIG. 2: The reweighting factors at $m = 0.1, 0.2, 0.3$ and $\beta = 1.0$.

III. THE CHIRAL CONDENSATIONS

We measure the chiral condensations $\langle \bar{\psi}\psi \rangle_{\beta, m}^Q$ and $\langle \bar{\psi}\gamma_5\psi \rangle_{\beta, m}^Q$ with the fixed topological charge. The total expectation values of them in the θ vacuum can be obtained by the following formula,

$$\begin{aligned} \langle \bar{\psi}\psi \rangle_{\beta, m}^{\theta} &= \frac{\sum_Q e^{iQ\theta} \langle \bar{\psi}\psi \rangle_{\beta, m}^Q R^Q(\beta, m)}{\sum_Q e^{iQ\theta} R^Q(\beta, m)}, \\ i\langle \bar{\psi}\gamma_5\psi \rangle_{\beta, m}^{\theta} &= \frac{\sum_Q e^{iQ\theta} i\langle \bar{\psi}\gamma_5\psi \rangle_{\beta, m}^Q R^Q(\beta, m)}{\sum_Q e^{iQ\theta} R^Q(\beta, m)}. \end{aligned} \quad (10)$$

In our practical calculation we truncate the sum over topological charge so that Q is restricted to be $|Q| \leq Q_{\max}$ where $Q_{\max} = 4$ for $m = 0.1, 0.15, 0.2$ and $Q_{\max} = 5$ for $m = 0.25, 0.3$. The scalar and the pseudoscalar operators

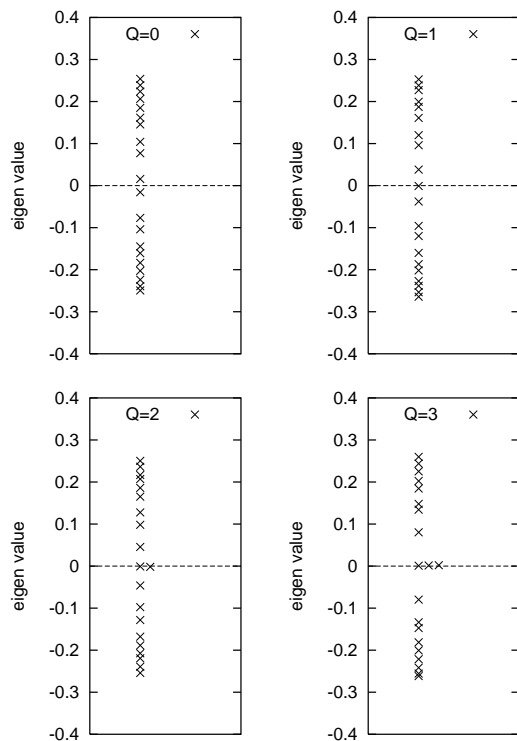


FIG. 3: The eigenvalues of the domain-wall Dirac operator $\gamma_5 D$ at $\beta = 1.0$ in each sector. The index theorem is realized very well.

are defined as

$$\begin{aligned}\bar{\psi}\psi(x) &= \bar{\psi}(x, L_s)\psi(x, 0) + \bar{\psi}(x, 0)\psi(x, L_s), \\ \bar{\psi}\gamma_5\psi(x) &= \bar{\psi}(x, L_s)\psi(x, 0) - \bar{\psi}(x, 0)\psi(x, L_s),\end{aligned}\quad (11)$$

where $L_s = 6$ denotes the size of the extra dimension of the domain-wall fermions. In order to increase the statistics, spatial averages are always taken for the expectation values of local operators.

The condensations in each topological sector $\langle\bar{\psi}\psi\rangle^Q$ and $\langle\bar{\psi}\gamma_5\psi\rangle^Q$ are plotted in Fig.4, where the numbers are given in Tables III, IV. It is obvious that the Q dependence of $\langle\bar{\psi}\psi\rangle^Q$ is symmetric and that of $\langle\bar{\psi}\gamma_5\psi\rangle^Q$ is anti-symmetric, which can be understood from parity symmetry. The topological charge dependence of $\langle\bar{\psi}\gamma_5\psi\rangle^Q$ can be explained from the chiral anomaly equation given as

$$\partial_\mu A^\mu = 2mi\bar{\psi}\gamma_5\psi + \frac{i}{2\pi}\epsilon^{\mu\nu}F_{\mu\nu}.\quad (12)$$

Taking expectation values in the fixed topological sector and making summations over the whole spacetime volume, one obtains the following relation

$$-\langle\bar{\psi}\gamma_5\psi\rangle^Q = Q/(mV),\quad (13)$$

which is in complete agreement with our lattice results. We also plot the ‘‘reweighted’’ condensations $\langle\bar{\psi}\psi\rangle^Q R^Q$ and $\langle\bar{\psi}\gamma_5\psi\rangle^Q R^Q$ in Fig.5. It is important to note that

most of the contributions in $i\langle\bar{\psi}\gamma_5\psi\rangle^{\theta\neq 0}$ come from $Q \neq 0$ sectors.

The fermion mass dependence of the total condensations $\langle\bar{\psi}\psi\rangle^{\theta=0}$ are presented in Fig.6 in which we also plot the fit function;

$$f(m) = Am^B.\quad (14)$$

Figure 6 also shows the prediction from the analytic result of the continuum theory in Eq.(1) using m_π^2 as an input

$$-\langle\bar{\psi}\psi\rangle = \frac{c_{\bar{\psi}\psi}}{c_\pi^2 m} m_\pi^2.\quad (15)$$

In the following analysis we adopt the value of $c_{\bar{\psi}\psi}/c_\pi^2 = 1/(4\pi)$ by Hetrick *et al.*[7]. We find that our lattice results give a good agreement with the analytic results, as was also the case in the previous lattice studies [10, 11, 12, 13, 14, 15, 16, 17, 18, 19].

We also present the θ dependences of the total condensations at $m = 0.15, 0.3$ as well as analytic results in Fig.7 and Fig.8. The numerical data are given in Tables V, VI. The qualitative features of the results in the continuum theory are realized in our simulation (See Eq.(1)). Our lattice results show 30 % deviations from the analytic results. Possible source of this discrepancies may be the discretization error or the error in the reweighting factor.

IV. THE η' MESON CORRELATORS AND THE CHIRAL CONDENSATIONS IN EACH TOPOLOGICAL SECTOR

The flavor singlet pseudoscalar meson η' is expected to be influenced by the topological properties of the vacuum. In QCD, the chiral anomaly gives a qualitative solution to the U(1) problem and it has been a long standing issue whether the mass gap between the flavor singlet and nonsinglet pseudoscalars can really be explained quantitatively from the lattice calculation. For this reason a number of unquenched lattice QCD simulations with $n_f = 2$ to observe the mass gap [30, 31, 32, 33] have been carried out.

The massive Schwinger model also has the mass gap between the flavor singlet and nonsinglet pseudoscalars due to the chiral anomaly. Since it is a two-dimensional theory, the numerical cost is much smaller than QCD and the disconnected diagrams can be evaluated explicitly without relying on the noise method [34] or the Kuramashi’s method [35]. The η' meson mass in $\theta = 0$ vacuum has been obtained using the overlap fermion [19].

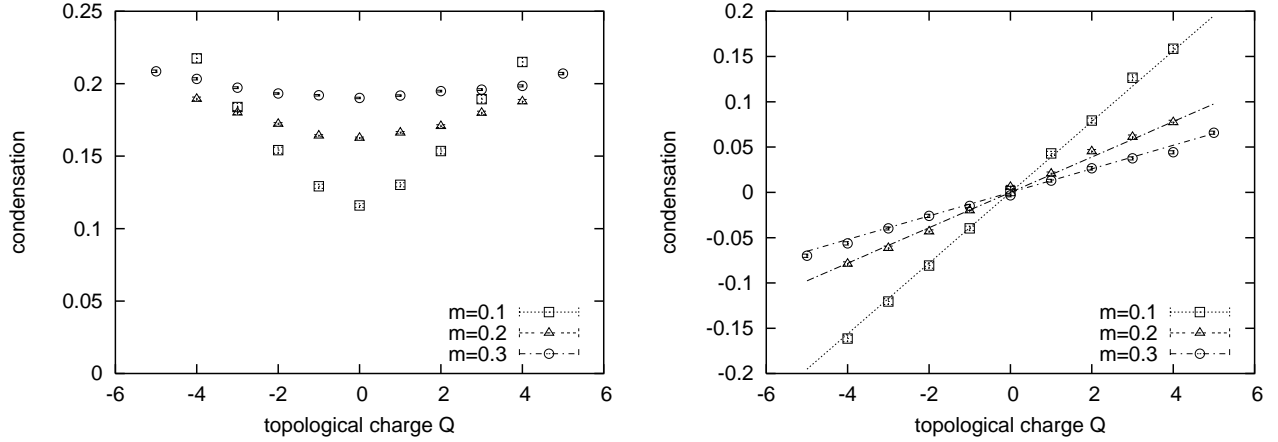


FIG. 4: **Left** : Lattice results of the condensation $-\langle \bar{\psi}\psi \rangle^Q$ at $\beta = 1.0$. It increases with $|Q|$ symmetrically. **Right** : Lattice results of the condensation $-\langle \bar{\psi}\gamma_5\psi \rangle^Q$ in each topological sector at $\beta = 1.0$. The lines show the prediction from the anomaly equation $-\langle \bar{\psi}\gamma_5\psi \rangle^Q = Q/(mV)$, which agrees with our data.

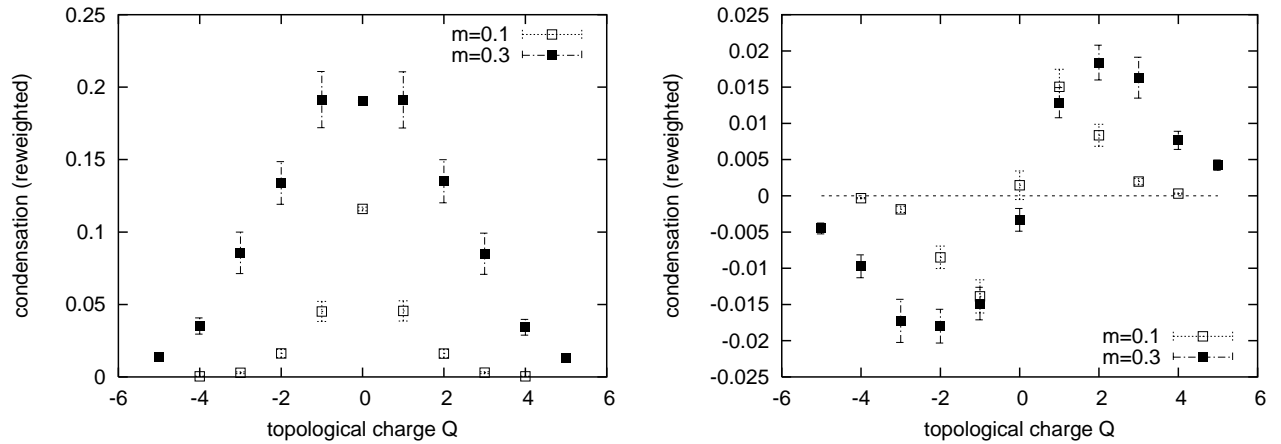


FIG. 5: **Left** : Reweighted condensation $-\langle \bar{\psi}\psi \rangle^Q R^Q$ in each topological sector at $\beta = 1.0$. **Right** : Reweighted condensation $-\langle \bar{\psi}\gamma_5\psi \rangle^Q R^Q$ in each topological sector at $\beta = 1.0$. Note that the largest contribution comes from $Q \neq 0$ sector.

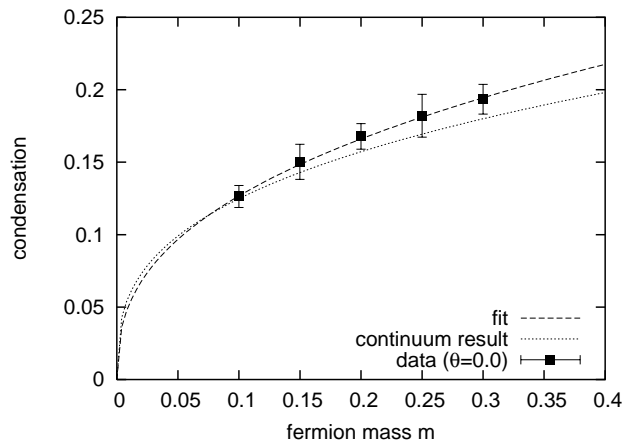


FIG. 6: The fermion mass dependence of $-\langle \bar{\psi}\psi \rangle^\theta$ at $\beta = 1.0$ and $\theta = 0$. The dashed line is the result of the fit with the function Am^B ($A = 0.311(36)$, $B = 0.388(68)$, $\chi^2/\text{dof} = 0.068$.) The index B is consistent with $B = 1/3$ in the continuum theory. The dotted line is the prediction of the condensation from the relation $-\langle \bar{\psi}\psi \rangle^\theta = c_{\bar{\psi}\psi} m_\pi^2 / c_\pi^2 m$ with our data of m_π in Table II and $c_{\bar{\psi}\psi} / c_\pi^2 = 1/(4\pi)$ by Hetrick *et al.* [7].

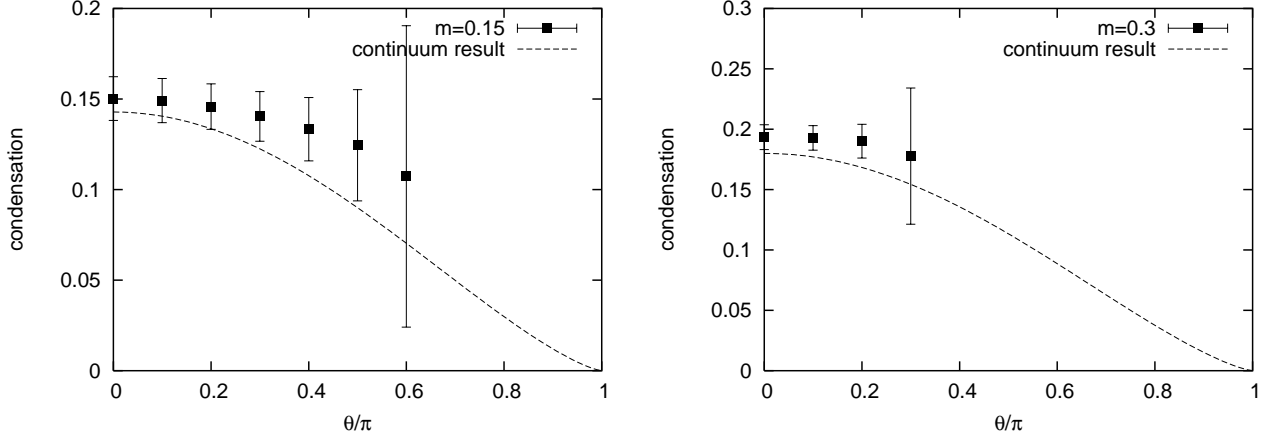


FIG. 7: The θ dependence of $-\langle\bar{\psi}\psi\rangle^\theta$ at $\beta = 1.0$ and $m = 0.15, 0.3$. The dashed line shows the continuum result $A \cos^{4/3} \frac{\theta}{2}$ where $A = 1/(4\pi)m_\pi^2$. **Left** : $m = 0.15$. **Right** : $m = 0.3$.

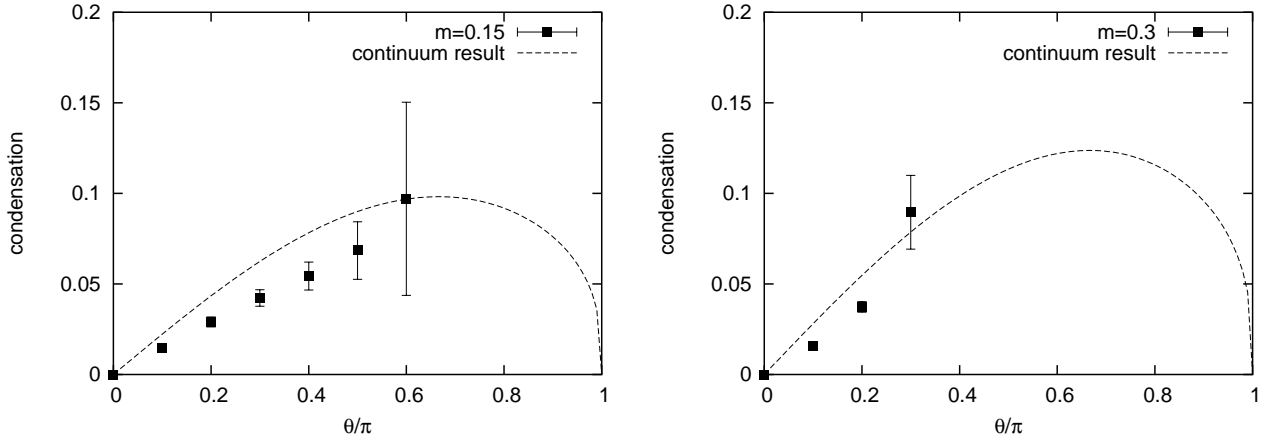


FIG. 8: The θ dependence of $i\langle\bar{\psi}\gamma_5\psi\rangle^\theta$ at $\beta = 1.0$ and $m = 0.15, 0.3$. The dashed line shows the continuum result $A \sin \frac{\theta}{2} \cos^{1/3} \frac{\theta}{2}$ where A is the same value of $-\langle\bar{\psi}\psi\rangle^\theta$. **Left** : $m = 0.15$. **Right** : $m = 0.3$.

The η' meson propagator is written as

$$\begin{aligned} & \langle \eta'^{\dagger}(x)\eta'(y) \rangle \\ &= \left\langle \left(-\sum_{f=1}^2 \bar{\psi}_f \gamma_5 \psi_f(x) \right) \left(\sum_{f=1}^2 \bar{\psi}_f \gamma_5 \psi_f(y) \right) \right\rangle \\ &= +2 \left\langle \text{tr} \left(\gamma_5 \frac{1}{D}(x, y) \gamma_5 \frac{1}{D}(y, x) \right) \right\rangle \\ &\quad - 4 \left\langle \text{tr} \left(\gamma_5 \frac{1}{D}(x, x) \right) \text{tr} \left(\gamma_5 \frac{1}{D}(y, y) \right) \right\rangle, \end{aligned} \quad (16)$$

where the second term is so-called disconnected part.

Fig.9 shows the propagators in each topological sector $\langle \eta'^{\dagger}(x)\eta'(0) \rangle^Q$. The result indicates the existence of long-range correlations. We evaluate them by fitting the data with the function

$$f(x) = A(e^{-Bx} + e^{-B(L-x)}) + C, \quad (17)$$

where $L = 16$ is the size of the lattice. We take $x \geq 3$ for the fitting range, we have also checked that the change

of the value of C for different fitting range is small (less than 5%).

The data of C in each topological sector are listed in Table VII. The results for $m = 0.1, 0.2, 0.3$ are also plotted in Fig.10. We find that there is a long-range correlation even in $Q = 0$ sector. Moreover, it is remarkable that it gives the largest contribution to the total expectation value in the θ vacuum.

We would like to explain this phenomenon by clustering properties. Consider the two operators put on $t = T/2$ and $t = -T/2$ as Fig.11. We expect that in the large volume limit the path integrals for the correlation functions in the volume V can be expressed in terms of the chiral condensations as follows,

$$\begin{aligned} & Z_V^Q \langle \eta'^{\dagger}(T/2)\eta'(-T/2) \rangle^Q \xrightarrow{T \rightarrow \infty} \\ & - \sum_{Q'} Z_{V_2}^{Q'} \langle \sum_f \bar{\psi}_f \gamma_5 \psi_f \rangle_B^{Q'} Z_{V_1}^{Q-Q'} \langle \sum_f \bar{\psi}_f \gamma_5 \psi_f \rangle_A^{Q-Q'}, \end{aligned} \quad (18)$$

where Z 's denote the partition functions and $\langle \rangle_{A,B}^{Q'}$ means

the expectation value in the region A, B with volume V_1, V_2 ($V = V_1 + V_2$) in which the gauge fields have a topological charge Q' in that region. In $Q = 0$ case taking $V_1 = V_2 = V/2$ we obtain

$$\begin{aligned} & Z_V^0 \langle \eta^\dagger(T/2)\eta'(-T/2) \rangle^{Q=0} \xrightarrow{T \rightarrow \infty} \\ & - \sum_{Q'} Z_{V/2}^{Q'} \langle \sum_f \bar{\psi}_f \gamma_5 \psi_f \rangle_B^{Q'} Z_{V/2}^{-Q'} \langle \sum_f \bar{\psi}_f \gamma_5 \psi_f \rangle_A^{-Q'} \\ & = + \sum_{Q'} (Z_{V/2}^{Q'})^2 \left(\langle \sum_f \bar{\psi}_f \gamma_5 \psi_f \rangle_A^{Q'} \right)^2 > 0, \end{aligned} \quad (19)$$

where we assume $Z_{V/2}^Q = Z_{V/2}^{-Q}$, $\langle O \rangle_A^Q = \langle O \rangle_B^Q$ and we use the anti-symmetry;

$$\langle \bar{\psi} \gamma_5 \psi \rangle^Q = -\langle \bar{\psi} \gamma_5 \psi \rangle^{-Q}, \quad (20)$$

as seen in Eq.(13) and Fig.4. Moreover, the Q dependence of the long-range correlations for large Q and the large volume limit can also be understood. In this limit, since Q, V are extensive quantities, the free energy $F(Q, V)$ defined as $F = -\ln(Z_V^Q)$ which is another extensive quantity should be expressed as

$$F = Vf \left(\frac{Q}{V} \right), \quad (21)$$

where f is some unknown function. Substituting Eq.(21) and approximating the sum over Q' by the integral over Q' , we obtain

$$\begin{aligned} & Z_V^Q \langle \eta^\dagger(T/2)\eta'(-T/2) \rangle^Q \xrightarrow{T \rightarrow \infty} \\ & - \int dQ' \frac{2(Q-Q')}{mV_1} \frac{2Q'}{mV_2} e^{-(V_1 f(\frac{Q-Q'}{V_1}) + V_2 f(\frac{Q'}{V_2}))}, \end{aligned} \quad (22)$$

where we use Eq.(13) (see also Fig.4). In the large volume limit, the integral over Q' is dominated by $Q'_* = \frac{QV_2}{V_1+V_2}$, which minimizes the total free energy. We can evaluate the integral by integrating the fluctuations of Q' around Q'_* . Changing variables as $Q' = Q'_* + q$ and expanding the free energy in q to the second order, right hand side of Eq.(22) becomes

$$- \int dq \frac{4}{m^2} \left(\frac{Q^2}{V^2} - \frac{q^2}{V_1 V_2} \right) e^{-(Vf(\frac{Q}{V}) + \frac{Vq^2}{2V_1 V_2} f''(\frac{Q}{V}))}, \quad (23)$$

where $V = V_1 + V_2$. Performing the integral over q to the first order we obtain

$$\langle \eta^\dagger(T/2)\eta'(-T/2) \rangle^Q \xrightarrow{T \rightarrow \infty} -\frac{4}{m^2} \left(\frac{Q^2}{V^2} - \frac{1}{V f''(\frac{Q}{V})} \right). \quad (24)$$

The second term is indeed suppressed in the limit where both Q and the volume becomes large as expected. In

Fig.10, we compare our lattice results on the Q dependence of the long-range correlation and the first term in Eq.(24). It is surprising that this argument describes the results in Fig.10 very well.

Thus we conclude that there is a relation between the long-range correlation of η' and the chiral condensations, which is understood by the clustering property of the theory based on the discussion of Q' instantons in the half of the space and $Q' - Q$ anti-instantons in the another half. Here we would like to emphasize two points;

- The η' meson has a long-range correlation in each topological sector even in $Q = 0$ case in spite of the fact that $\langle \bar{\psi} \gamma_5 \psi \rangle^{Q=0}$ vanishes.
- Our lattice data at large Q satisfy the following relation,

$$\langle \eta^\dagger(\infty)\eta'(0) \rangle_V^Q \sim -\frac{4}{m^2} \frac{Q^2}{V^2}, \quad (25)$$

which can be explained by the clustering property.

V. THE η' MESON IN THE θ VACUUM

From the discussion in section IV, we expect that the correlation of the η' meson in the θ vacuum is expressed by the following function,

$$\langle \eta^\dagger(x)\eta'(0) \rangle^\theta = A(e^{-m_{\eta'} x} + e^{-m_{\eta'}(L-x)}) + C_\theta. \quad (26)$$

We plot the data of $\langle \eta^\dagger(x)\eta'(0) \rangle^\theta$ at $\theta = 0, 0.3\pi, m = 0.1$ in the left of Fig.12. Fitting the data with Eq.(26), we evaluate the η' meson mass and the long-range correlation C_θ . The fitting range is determined as $x > 2$ from the effective mass at $\theta = 0$ (See Fig.12).

As Fig.13 and Table VIII show, the qualitative feature of the long-range correlations is consistent with $4|\langle \bar{\psi} \gamma_5 \psi \rangle^\theta|^2$ at small m . Especially it is remarkable that our data show the cancellation of the long-range correlations in the $\theta = 0$ vacuum at $m = 0.1, 0.15$. On the other hand, we find that it is difficult to evaluate them precisely as m increases since the Q dependence the operator is steep ($\propto Q^2$). In fact, the long-range correlation at $m = 0.2$ gives 3.5 σ deviation from zero. This is because one gets contributions from larger number of topological sectors as shown in Fig.10 so that the cancellation becomes more delicate. Obviously the present level of accuracies for the reweighting factors R^Q and the condensation $\langle \bar{\psi} \gamma_5 \psi \rangle$ are not sufficient for larger masses. Moreover, at $m = 0.25, 0.3$ the sectors with $|Q| > |Q_{\max}|$ cannot be ignored. In order to have a good control of the long-range correlation for larger masses, one has to reduce the statistical or systematic errors of R^Q and $\langle \bar{\psi} \gamma_5 \psi \rangle$, while also evaluating higher topological sectors.

The data of the η' meson mass are presented in Fig.14. They have large statistical errors but we find that the η' meson is indeed heavier than the pion as predicted by the continuum theory.

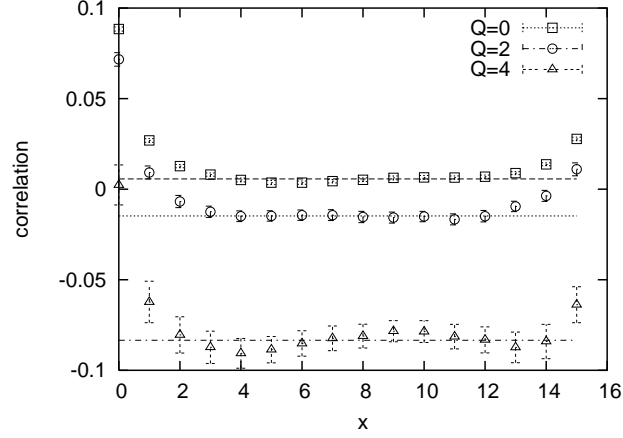


FIG. 9: The propagators of the η' meson in each topological sector at $\beta = 1.0$ and $m = 0.1$. Long-range correlations are seen. The lines are the results of the fit with the function in Eq.(17).

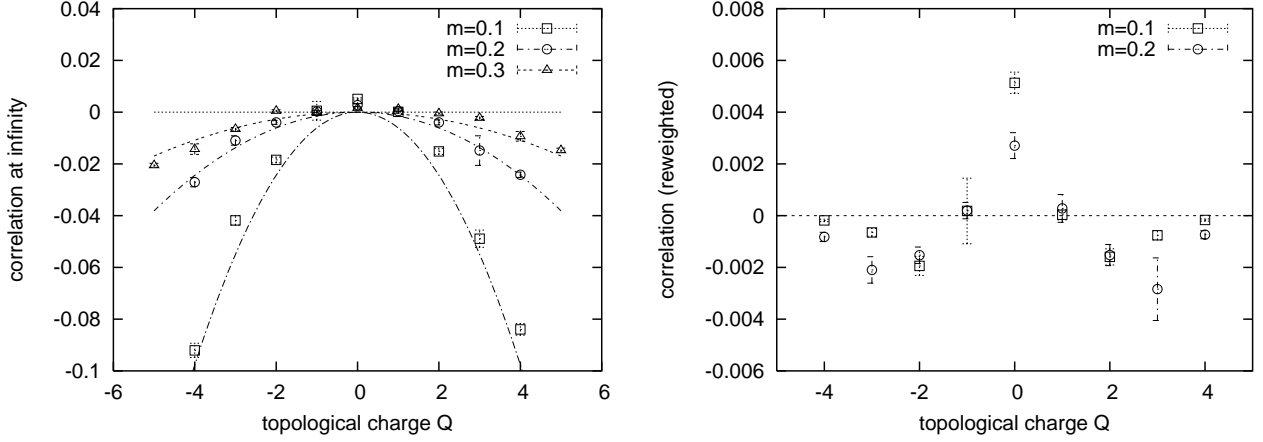


FIG. 10: **Left** : The long-range correlations in each topological sector $\langle \eta'^{\dagger}(\infty)\eta'(0) \rangle^Q$. The lines show the Q dependence for large Q derived from the clustering property $\langle \eta'^{\dagger}(\infty)\eta'(0) \rangle^Q = -4Q^2/(mV)^2$, which agrees with our data quite well. **Right** : The long-range correlations (reweighted) $\langle \eta'^{\dagger}(\infty)\eta'(0) \rangle^Q R^Q$. It is interesting that the long-range correlation of $Q = 0$ sector is non-zero and gives the largest contribution to the total expectation value in the θ vacuum.

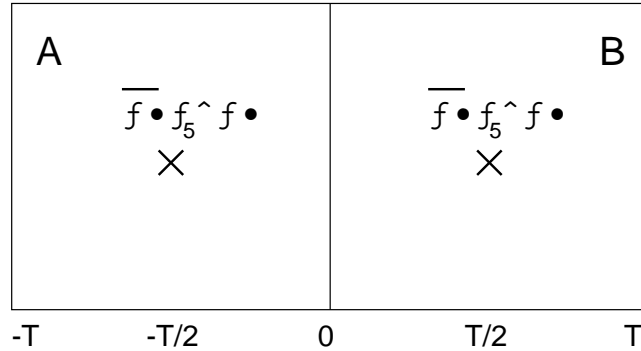


FIG. 11: The long-range correlation of the η' meson can be understood as a summation of the products of the condensations which are determined by the topological charge in the region A and B respectively; $Z_V^Q \langle \eta'^{\dagger}(T/2)\eta'(-T/2) \rangle^Q \rightarrow_{T \rightarrow \infty} -\sum_{Q'} Z_{V_2}^{Q'} \langle \bar{\psi}_f \gamma_5 \psi_f \rangle_B^{Q'} Z_{V_1}^{Q-Q'} \langle \bar{\psi}_f \gamma_5 \psi_f \rangle_A^{Q-Q'}$

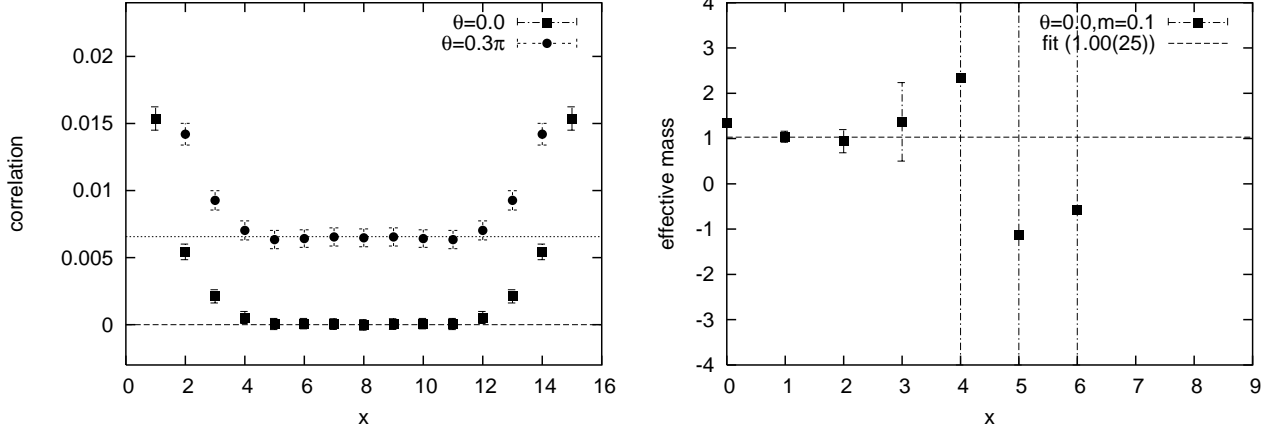


FIG. 12: **Left** : The propagations of the η' meson at $\theta = 0, 0.3\pi$ and $m = 0.1$ are shown. The lines show C_θ in Eq.(26). It is obvious that there are long-range correlations at $\theta \neq 0$. On the other hand, $\theta = 0$ case is consistent with zero. **Right** : The effective mass plot of the η' meson at $\theta = 0$ and $m = 0.1$. The dashed line shows the result of the fit in Eq.(26). The fitting range is $x \geq 2$.

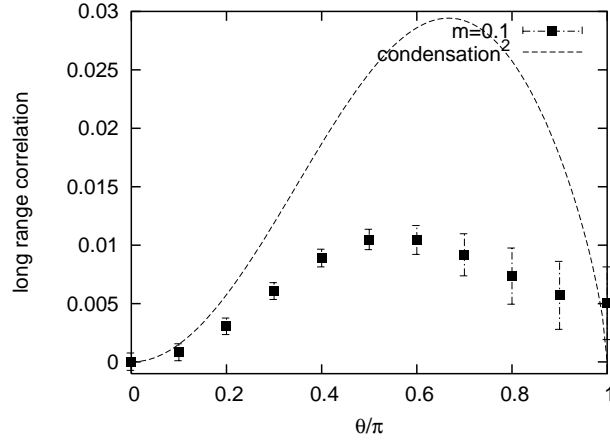


FIG. 13: The long-range correlations of the η' meson in the θ vacuum $\langle \eta'^{\dagger}(\infty)\eta'(0) \rangle^\theta$. The dashed line shows the result of $4|\langle \bar{\psi}\gamma_5\psi \rangle^\theta|^2$ in the continuum theory.

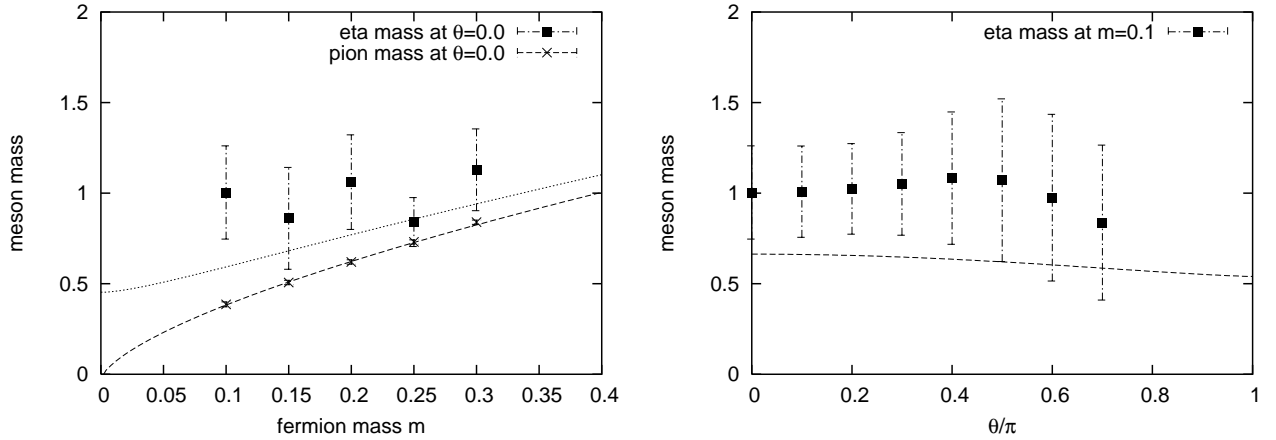


FIG. 14: **Left** : The η' meson mass and the pion mass at $\theta = 0$. The lines show the continuum results from Hosotani et.al [9] in which the effective coupling constant $g_{\text{eff}} = 0.68$ is determined from the pion mass at $m = 0.1$ and $\theta = 0$. **Right** : The θ dependence of the η' meson at $m = 0.1$.

VI. SUMMARY AND DISCUSSION

We investigate the chiral condensations and the η' meson propagators in each topological sector and in the θ vacuum. Let us summarize the results as follows.

1. The chiral condensations are nonzero in each sector,

$$\begin{aligned} & -\langle \bar{\psi}\psi \rangle^Q \neq 0 \quad (\text{Q symmetric}) \\ -\langle \bar{\psi}\gamma_5\psi \rangle^Q &= \frac{Q}{mV} \neq 0 \quad (\text{Q anti-symmetric}), \end{aligned} \quad (27)$$

where the second equation is consistent with the anomaly equation. The total expectation values in the θ vacuum obtained by the reweighting method are qualitatively consistent with the results of the continuum theory.

2. There actually exist the long-range correlations of the η' meson in each sector,

$$\langle \eta'^{\dagger}(\infty)\eta'(0) \rangle^Q \neq 0, \quad (28)$$

even in $Q = 0$ case. It is also remarkable that our data show the following Q dependence of the long-range correlation as

$$\begin{aligned} & \langle \eta'^{\dagger}(\infty)\eta'(0) \rangle^{Q=0} > 0, \\ \langle \eta'^{\dagger}(\infty)\eta'(0) \rangle^{Q>2} &\sim -\frac{4Q^2}{m^2V^2} < 0, \end{aligned} \quad (29)$$

which can be explained by the clustering property. This means that the precise measurements of higher topological sectors are necessary to cancel the long-range correlation in the total expectation value at $\theta = 0$.

3. Thus the η' meson correlations in the θ vacuum should be treated as the following function,

$$\langle \eta'^{\dagger}(x)\eta'(0) \rangle^{\theta} = A(e^{-m_{\eta'}x} + e^{-m_{\eta'}(L-x)}) + C_{\theta}, \quad (30)$$

even in the $\theta = 0$ vacuum. Our results of C_{θ} and $m_{\eta'}$ from the fit are qualitatively consistent with the continuum results as $\langle \eta'^{\dagger}(\infty)\eta'(0) \rangle^{\theta} \propto |\langle \bar{\psi}\gamma_5\psi \rangle^{\theta}|^2$, although there are discrepancies at the quantitative level.

It is now clear why the contribution from “disconnected” diagrams is very noisy. It is because each configuration gives the pseudoscalar condensation. They must be canceled at $\theta = 0$ by parity symmetry. We should however take the existence into account since our simulation would have both of the systematic and statistical errors in the evaluation of the higher topological sectors. Note that 4-dimensional QCD might have the same problems. It would be also important to investigate the topological effects on the $\bar{\psi}\gamma_5\psi$ condensation and the η' meson propagations in QCD.

It should be stressed that the present lattice formalism of the chiral fermion already allows us to study the topological effects as a well defined problem in principle. Although our method may be limited to two dimensions, it would be important to investigate some new efficient method or algorithm for the study of the topological effect in QCD.

ACKNOWLEDGMENTS

The authors would like to thank H. Matsufuru, T. Umeda, Y. Kikukawa, S.Hashimoto, Y.Aoki, K. Takahashi and T. Takimi for useful discussions and comments. The author also express special thanks to T. Izubuchi for crucial discussions on the relation between the chiral condensation and the anomaly equation. They would also like to acknowledge M. Hamanaka and S. Sugimoto for informing us of the analytic results on instantons and the massive Schwinger model. The authors thank the Yukawa Institute for Theoretical Physics at Kyoto University, where this work was initiated during the YITP-W-02-15 on “YITP School on Lattice Field Theory”. The numerical simulations were done on NEC SX-5 at Research Center for Nuclear Physics in Osaka University, and Hitachi SR8000 model F1 supercomputer at KEK. This work was supported in part by Grant-in-Aid for Scientific Research from the Ministry of Education, Culture, Sports, Science and Technology of Japan (No.13135213).

They would also like to thank to YITP members for constant encouragements.

APPENDIX

In this appendix, we present our results of the topological susceptibility χ defined as

$$\chi \equiv \frac{1}{V} \langle Q^2 \rangle. \quad (31)$$

The topological susceptibility is a useful measure of the topological fluctuations of the vacuum, which is extensively studied in QCD [36, 37, 38, 39, 40, 41, 42, 43, 44].

Fig.15 indeed shows a mass dependence of χ which decreases towards the chiral limit somewhat faster than linearly in m . It would be interesting to compare it with the analytical results. Recently, the topological susceptibility was also studied using the overlap fermion and staggered fermion [10], where they find χ decreases slower than linearly in m when the Leutwyler-Smilga parameter $x \equiv V\Sigma m$ is large.

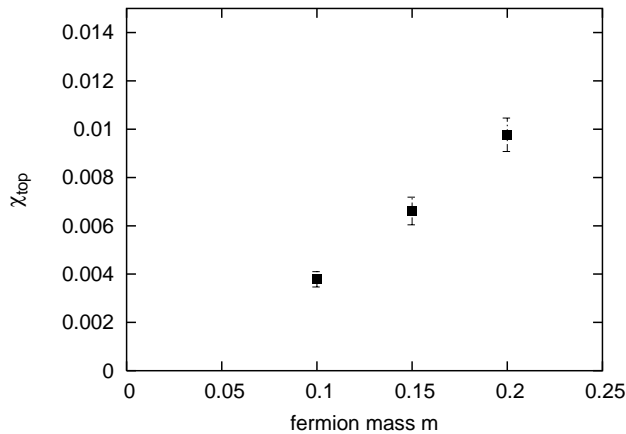


FIG. 15: The mass dependence of the topological susceptibility χ

-
- [1] P. H. Ginsparg and K. G. Wilson, Phys. Rev. D **25**, 2649 (1982).
- [2] H. Fukaya and T. Onogi, Phys. Rev. D **68**, 074503 (2003).
- [3] J. S. Schwinger, Phys. Rev. **128**, 2425 (1962).
- [4] S. R. Coleman, R. Jackiw and L. Susskind, Annals Phys. **93**, 267 (1975).
- [5] S. R. Coleman, Annals Phys. **101**, 239 (1976).
- [6] A. V. Smilga, Phys. Rev. D **55**, 443 (1997).
- [7] J. E. Hetrick, Y. Hosotani and S. Iso, Phys. Lett. B **350**, 92 (1995).
- [8] R. Rodriguez and Y. Hosotani, Phys. Lett. B **375**, 273 (1996).
- [9] Y. Hosotani and R. Rodriguez, J. Phys. A **31**, 9925 (1998).
- [10] S. Dürr and C. Hoelbling, arXiv:hep-lat/0311002.
- [11] S. Dürr, Phys. Rev. D **62**, 054502 (2000).
- [12] S. Elser, arXiv:hep-lat/0103035.
- [13] S. Elser and B. Bunk, Nucl. Phys. Proc. Suppl. **53**, 953 (1997).
- [14] J. Kiskis and R. Narayanan Phys. Rev. D **62**, 054501 (2000).
- [15] S. Chandrasekharan, Phys. Rev. D **59**, 094502 (1999).
- [16] C. Gattringer, Phys. Rev. D **53**, 5090 (1996).
- [17] P. de Forcrand, J. E. Hetrick, T. Takaishi and A. J. van der Sijs, Nucl. Phys. Proc. Suppl. **63** (1998) 679.
- [18] P. M. Vranas, Phys. Rev. D **57**, 1415 (1998).
- [19] L. Giusti, C. Hoelbling and C. Rebbi, Phys. Rev. D **64**, 054501 (2001).
- [20] U. J. Wiese, Nucl. Phys. B **318**, 153 (1989).
- [21] A. S. Hassan, M. Imachi and H. Yoneyama, Prog. Theor. Phys. **93**, 161 (1995).
- [22] A. S. Hassan, M. Imachi, N. Tsuzuki and H. Yoneyama, Prog. Theor. Phys. **94**, 861 (1995).
- [23] M. Imachi, T. Kakitsuka, N. Tsuzuki and H. Yoneyama, arXiv:hep-lat/9702018.
- [24] J. C. Plefka and S. Samuel, Phys. Rev. D **56**, 44 (1997).
- [25] V. Azcoiti, G. Di Carlo, A. Galante and V. Laliena, Phys. Rev. Lett. **89**, 141601 (2002).
- [26] M. D'Elia, Nucl. Phys. B **661**, 139 (2003).
- [27] M. Lüscher, Nucl. Phys. B **549**, 295 (1999).
- [28] D. B. Kaplan, Phys. Lett. B **288**, 342 (1992).
- [29] Y. Shamir, Nucl. Phys. B **406**, 90 (1993).
- [30] V. Furman and Y. Shamir, Nucl. Phys. B **439**, 54 (1995).
- [31] L. Venkataraman and G. Kilcup, arXiv:hep-lat/9711006.
- [32] C. McNeile and C. Michael [UKQCD Collaboration], Phys. Lett. B **491**, 123 (2000) [Erratum-ibid. B **551**, 391 (2003)].
- [33] T. Struckmann *et al.* [TXL Collaboration], Phys. Rev. D **63**, 074503 (2001).
- [34] V. I. Lesk *et al.* [CP-PACS Collaboration], Phys. Rev. D **67**, 074503 (2003).
- [35] K. Bitar *et al.*, Nucl. Phys. **B313**, 348 (1989).
- [36] H. R. Fiebig and R. M. Woloshyn, Phys. Rev. D **42**, 3520 (1990).
- [37] Y. Kuramashi *et al.*, Phys. Rev. Lett. **72**, 3448 (1994).
- [38] M. Fukugita *et al.*, Phys. Rev. D **51**, 3952 (1995).
- [39] H. Gausterer, J. Potvin, S. Sanielevici and P. Woit, Phys. Lett. B **233**, 439 (1989).
- [40] K. M. Bitar *et al.*, Phys. Rev. D **44**, 2090 (1991).
- [41] Y. Kuramashi, M. Fukugita, H. Mino, M. Okawa and A. Ukawa, Phys. Lett. B **313**, 425 (1993).
- [42] A. Hart and M. Teper [UKQCD Collaboration], Phys. Lett. B **523**, 280 (2001).
- [43] G. S. Bali *et al.* [TXL Collaboration], Phys. Rev. D **64**, 054502 (2001).
- [44] A. Hasenfratz, Phys. Rev. D **64**, 074503 (2001).
- [45] B. Alles, M. D'Elia and A. Di Giacomo, Phys. Lett. B **483**, 139 (2000).
- [46] C. Bernard *et al.*, Phys. Rev. D **68**, 114501 (2003).
- [47] UKQCD and A. Hart [QCDSF Collaborations], arXiv:hep-lat/0401015.

	$m = 0.1$	$m = 0.15$	$m = 0.2$	$m = 0.25$	$m = 0.3$
R^0	1.000(0)	1.000(0)	1.000(0)	1.000(0)	1.000(0)
R^1	0.349(53)	0.74(12)	0.652(74)	0.78(14)	0.99(10)
R^2	0.105(19)	0.295(47)	0.384(42)	0.63(11)	0.693(76)
R^3	0.0154(34)	0.060(10)	0.191(34)	0.285(51)	0.434(72)
R^4	0.00199(51)	0.0166(46)	0.0304(62)	0.129(25)	0.173(27)
R^5			0.00317(63)	0.0346(70)	0.064(11)

TABLE I: The reweighting factors $R^Q(\beta, m)$ at $\beta = 1.0$ for various topological sectors and the fermion masses.

pion mass	
$m = 0.1$	0.386(14)
$m = 0.15$	0.507(13)
$m = 0.2$	0.620(12)
$m = 0.25$	0.730(12)
$m = 0.3$	0.840(12)

TABLE II: The pion mass at $\beta = 1.0$ and $\theta = 0$.

	$m = 0.1$	$m = 0.15$	$m = 0.2$	$m = 0.25$	$m = 0.3$
$-\langle\bar{\psi}\psi\rangle^0$	0.1160(13)	0.14324(85)	0.16251(68)	0.17861(56)	0.19018(48)
$-\langle\bar{\psi}\psi\rangle^1$	0.1302(14)	0.14709(99)	0.16619(78)	0.17839(60)	0.19181(52)
$-\langle\bar{\psi}\psi\rangle^{-1}$	0.1292(14)	0.14852(95)	0.16407(71)	0.17992(65)	0.19200(51)
$-\langle\bar{\psi}\psi\rangle^2$	0.1535(20)	0.1591(12)	0.17068(97)	0.18208(68)	0.19490(58)
$-\langle\bar{\psi}\psi\rangle^{-2}$	0.1541(21)	0.1611(14)	0.17223(84)	0.18314(63)	0.19326(55)
$-\langle\bar{\psi}\psi\rangle^3$	0.1894(26)	0.1758(15)	0.1798(12)	0.18760(87)	0.19592(62)
$-\langle\bar{\psi}\psi\rangle^{-3}$	0.1839(25)	0.1805(18)	0.1800(13)	0.19051(89)	0.19725(62)
$-\langle\bar{\psi}\psi\rangle^4$	0.2150(30)	0.1912(18)	0.1877(15)	0.19526(98)	0.19848(68)
$-\langle\bar{\psi}\psi\rangle^{-4}$	0.2175(29)	0.1933(18)	0.1895(13)	0.19429(98)	0.20334(78)
$-\langle\bar{\psi}\psi\rangle^5$				0.2040(12)	0.20702(83)
$-\langle\bar{\psi}\psi\rangle^{-5}$				0.2030(11)	0.20857(87)

TABLE III: The scalar condensation $-\langle\bar{\psi}\psi\rangle^Q$ for a fixed topological charge Q at $\beta = 1.0$.

	$m = 0.1$	$m = 0.15$	$m = 0.2$	$m = 0.25$	$m = 0.3$
$-\langle\bar{\psi}\gamma_5\psi\rangle^0$	0.0014(20)	0.0001(19)	0.0058(18)	0.0045(19)	-0.0033(16)
$-\langle\bar{\psi}\gamma_5\psi\rangle^1$	0.0430(23)	0.0263(22)	0.0205(20)	0.0125(18)	0.0129(16)
$-\langle\bar{\psi}\gamma_5\psi\rangle^{-1}$	-0.0396(25)	-0.0288(20)	-0.0200(19)	-0.0181(18)	-0.0149(17)
$-\langle\bar{\psi}\gamma_5\psi\rangle^2$	0.0794(28)	0.0528(22)	0.0452(20)	0.0303(18)	0.0265(17)
$-\langle\bar{\psi}\gamma_5\psi\rangle^{-2}$	-0.0807(30)	-0.0584(23)	-0.0433(20)	-0.0349(17)	-0.0260(18)
$-\langle\bar{\psi}\gamma_5\psi\rangle^3$	0.1266(33)	0.0834(25)	0.0611(23)	0.0469(20)	0.0376(17)
$-\langle\bar{\psi}\gamma_5\psi\rangle^{-3}$	-0.1205(32)	-0.0896(26)	-0.0616(24)	-0.0524(20)	-0.0398(17)
$-\langle\bar{\psi}\gamma_5\psi\rangle^4$	0.1586(36)	0.1067(27)	0.0773(23)	0.0670(19)	0.0443(18)
$-\langle\bar{\psi}\gamma_5\psi\rangle^{-4}$	-0.1613(36)	-0.1094(28)	-0.0789(23)	-0.0637(20)	-0.0563(18)
$-\langle\bar{\psi}\gamma_5\psi\rangle^5$				0.0828(22)	0.0659(17)
$-\langle\bar{\psi}\gamma_5\psi\rangle^{-5}$				-0.0828(20)	-0.0700(18)

TABLE IV: The pseudoscalar condensation $-\langle\bar{\psi}\gamma_5\psi\rangle^Q$ for a fixed topological charge Q at $\beta = 1.0$.

	$m = 0.1$	$m = 0.15$	$m = 0.2$	$m = 0.25$	$m = 0.3$
$-\langle\bar{\psi}\psi\rangle^{\theta=0}$	0.1338(93)	0.150(12)	0.1678(88)	0.182(15)	0.193(10)
$-\langle\bar{\psi}\psi\rangle^{\theta=0.1\pi}$	0.1309(90)	0.149(12)	0.1667(87)	0.181(15)	0.193(10)
$-\langle\bar{\psi}\psi\rangle^{\theta=0.2\pi}$	0.1219(87)	0.146(13)	0.1632(97)	0.177(19)	0.190(14)
$-\langle\bar{\psi}\psi\rangle^{\theta=0.3\pi}$	0.107(10)	0.140(14)	0.155(17)	0.166(47)	0.178(56)

TABLE V: The scalar condensation $-\langle\bar{\psi}\psi\rangle^\theta$ in θ vacuum at $\beta = 1.0$.

	$m = 0.1$	$m = 0.15$	$m = 0.2$	$m = 0.25$	$m = 0.3$
$i\langle\bar{\psi}\gamma_5\psi\rangle^{\theta=0}$	0.0(0)	0.0(0)	0.0(0)	0.0(0)	0.0(0)
$i\langle\bar{\psi}\gamma_5\psi\rangle^{\theta=0.1\pi}$	0.0122(10)	0.0147(28)	0.0166(12)	0.0180(16)	0.0159(11)
$i\langle\bar{\psi}\gamma_5\psi\rangle^{\theta=0.2\pi}$	0.0229(20)	0.0290(46)	0.0343(25)	0.0398(42)	0.0373(29)
$i\langle\bar{\psi}\gamma_5\psi\rangle^{\theta=0.3\pi}$	0.0306(28)	0.0422(77)	0.0521(49)	0.0739(16)	0.090(15)

TABLE VI: The pseudoscalar condensation $i\langle\bar{\psi}\gamma_5\psi\rangle^\theta$ in θ vacuum at $\beta = 1.0$.

	$m = 0.1$	$m = 0.2$	$m = 0.3$
$\langle\eta^\dagger(\infty)\eta(0)\rangle^0$	0.00513(41)	0.00271(50)	0.00162(36)
$\langle\eta^\dagger(\infty)\eta(0)\rangle^1$	0.00010(56)	0.00043(82)	0.00119(43)
$\langle\eta^\dagger(\infty)\eta(0)\rangle^{-1}$	0.0005(36)	0.00030(48)	-0.07e-3(63)
$\langle\eta^\dagger(\infty)\eta(0)\rangle^2$	-0.0151(12)	-0.00397(97)	-0.49e-3(54)
$\langle\eta^\dagger(\infty)\eta(0)\rangle^{-2}$	-0.0184(11)	-0.00399(71)	0.48e-3(44)
$\langle\eta^\dagger(\infty)\eta(0)\rangle^3$	-0.0489(33)	-0.0149(57)	-0.00224(59)
$\langle\eta^\dagger(\infty)\eta(0)\rangle^{-3}$	-0.0418(19)	-0.0110(18)	-0.00658(68)
$\langle\eta^\dagger(\infty)\eta(0)\rangle^4$	-0.0839(23)	-0.0242(10)	-0.0093(19)
$\langle\eta^\dagger(\infty)\eta(0)\rangle^{-4}$	-0.0921(27)	-0.0271(18)	-0.0143(20)
$\langle\eta^\dagger(\infty)\eta(0)\rangle^5$			-0.01476(84)
$\langle\eta^\dagger(\infty)\eta(0)\rangle^{-5}$			-0.02055(79)

TABLE VII: The long-range correlation $\langle\eta^\dagger(\infty)\eta(0)\rangle^Q$ at $\beta = 1.0$ and $m = 0.1, 0.2, 0.3$. in each topological sector.

	$m = 0.1$	$m = 0.15$	$m = 0.2$
$\langle\eta^\dagger(\infty)\eta(0)\rangle^{\theta=0}$	0.03e-3(74)	-0.92e-3(46)	-0.00181(48)
$\langle\eta^\dagger(\infty)\eta(0)\rangle^{\theta=0.1\pi}$	0.83e-3(72)	-0.91e-3(43)	-0.87e-3(38)
$\langle\eta^\dagger(\infty)\eta(0)\rangle^{\theta=0.2\pi}$	0.00304(71)	0.00238(47)	0.00232(42)
$\langle\eta^\dagger(\infty)\eta(0)\rangle^{\theta=0.3\pi}$	0.00607(72)	0.00630(75)	0.0089(16)
$\langle\eta^\dagger(\infty)\eta(0)\rangle^{\theta=0.4\pi}$	0.00889(75)	0.0112 (15)	0.0180(45)
$\langle\eta^\dagger(\infty)\eta(0)\rangle^{\theta=0.5\pi}$	0.01048(88)	0.0171 (35)	0.0143(49)

TABLE VIII: The long-range correlation $\langle\eta^\dagger(\infty)\eta(0)\rangle^\theta$ at $\beta = 1.0$ and $m = 0.1, 0.15, 0.2$.